Contribution from the Corporate Research Science Laboratories,
Exxon Research and Engineering Company, Annandale, New Jersey 08801

Electronic Structure of MoS_4^{2-} and $Mo_3S_9^{2-}$

J. BERNHOLC* and E. I. STIEFEL*

Received June 11, 1984

We have carried out first-principles, self-consistent calculations for the MoS_4^{2-} and $Mo_3S_9^{2-}$ anions. The $Mo_3S_9^{2-}$ ion consists of a central square-pyramidal Mo coordinated by a terminal S and two chelating MoS_4^{2-} ligands. Bonding properties, charge distributions, individual electronic levels, and optical absorption spectra are discussed in detail. For MoS_4^{2-}, the ordering of levels agrees with previous calculations, but the energy positions of the levels necessitate a reassignment of the higher absorption bands. For $Mo_3S_9^{2-}$, the end molybdenum atoms are found to be Mo(VI) while the central Mo is Mo(IV), in agreement with the intuitive assignment. The MoS_4^{2-} fragments in the system serve both as electron donors through the bridging sulfur atoms and as electron acceptors by withdrawing electron density from the central molybdenum atom into the empty MoS_4^{2-} 4d levels. In both systems, the closeness of the atomic energy levels of the sulfur atom's 3p and the molybdenum atom's 4d and 5s levels results in substantial delocalization of the molecular orbitals. Nominally nonbonding sulfur atoms (at 3–3.5 Å) still interact sufficiently to split some of their bonding and antibonding levels by 0.7 eV. Both the bonding and the antibonding levels are occupied, however, leading to no net S–S bonding. The general ordering of levels is as follows: the lowest are the metal–sulfur bonding levels, followed by weakly S–S bonding sulfur levels, and finally by weakly S–S antibonding levels and nominally nonbonding Mo d orbitals (if present). The lowest unoccupied molecular orbitals are the metal–sulfur π^* antibonding levels.

I. Introduction

Molybdenum–sulfur complexes serve as synthetic models for molybdoenzyme active sites[1] and for hydrodesulfurization (HDS) and hydrodenitrogenation (HDN) catalysts.[2] Our ultimate goal is to provide an electronic structural understanding for these phenomena. To this end, we have undertaken detailed theoretical studies of several Mo–S compounds using first-principles techniques. In the present paper we focus on the anions MoS_4^{2-} and $Mo_3S_9^{2-}$.

The thiomolybdate anion, MoS_4^{2-}, plays an important role in the synthesis of various Mo–S systems.[1,3,4] It is one of the most versatile and active reagents in Mo–S solution chemistry[3] and plays a potentially key role in a number of biological processes. Only semiempirical[5] and Xα calculations[6,7] have been performed for this system.

$Mo_3S_9^{2-}$ was recently synthesized by the thermal reaction of MoS_4^{2-} in DMF solution under anaerobic conditions.[4] This anion formally consists of two MoS_4^{2-} groups, each chelating a central MoS^{2+} ion. As such, it contains MoS_4^{2-} as a chelating group and the electronic structure calculations of $Mo_3S_9^{2-}$ give us the opportunity to look at the manner in which MoS_4^{2-} serves as a ligand. To our knowledge, no other calculations have been reported for related MoS_4^{2-}-ligated systems.

In the present paper, we use theoretical results to examine bonding properties and charge distribution and discuss in detail the molecular orbitals of both MoS_4^{2-} and $Mo_3S_9^{2-}$. The highest occupied and the lowest unoccupied orbitals, which are most likely to serve as donor and acceptor orbitals in chemical reactions, respectively, are identified and described in terms of their orbital content. Our theoretical results agree well with XPS data[8] and are used to analyze the optical absorption spectrum.[4,9]

We have used the local density pseudopotential method,[10] which has its origins in solid-state physics. In this method the electrons are represented by effective one-electron wave functions. The "average" exchange and correlation contributions are included via a one-electron exchange-correlation potential. The interpretation of the results is thus as simple as in the extended Hückel theory.[11] The method is, however, first principles and parameter free.

The local density theory (LDT) accurately describes ground-state properties such as bond lengths, binding energies, or vibrational frequencies.[12] The optical absorption, however, involves excitation of an electron from the ground state to a higher excited state. Experience in solid-state physics shows that energies of the lowest excitations are underestimated by the local density theory.[13] Our calculated transitions energies will therefore be too low, compared to the experimental values. The general ordering of the various transitions is, however, correctly predicted by the LDT.

First-principles pseudopotentials (effective core potentials) are used to represent the core electrons. Therefore, only valence electrons explicitly enter the calculations. This procedure does not induce any loss of computational accuracy. Relativistic corrections, which are important for the inner core electrons of heavy atoms, are also included. In the present method, heavy atoms are treated as easily as the first-row atoms and relatively large molecules can be handled.

Our computational method has been extensively tested on several well-understood diatomic molecules.[10,14] Results were in good agreement both with experimental data and with other all-electron calculations. The method has even proven capable of treating multiply metal–metal-bonded (antiferromagnetically coupled) transition-metal systems.[14]

This paper is organized as follows: In section II we give a brief account of the method. In sections III and IV, respectively, we describe results for MoS_4^{2-} and $Mo_3S_9^{2-}$. In section V we present the Summary and Conclusions.

II. Calculations

In this section we outline briefly the theory and the computational procedures used in the present work. A full discussion may be found in ref 10.

(1) (a) E. I. Stiefel in "Molybdenum and Molybdenum-Containing Enzymes", M. P. Coughlan, Ed., Pergamon Press, New York, 1980; (b) J. T. Spence, *Coord. Chem. Rev.*, **48**, 59 (1983); (c) R. H. Holm, *Chem. Soc. Rev.*, **10**, 454 (1981); (d) B. A. Averill, *Struct. Bonding (Berlin)*, **53**, 59 (1983); (e) D. Coucouvanis, *Acc. Chem. Res.*, **14**, 201 (1981).
(2) (a) E. I. Stiefel, Proceedings of the Climax Fourth International Conference on the Chemistry and Uses of Molybdenum, H. F. Barry and P. C. H. Mitchell, Eds., Climax Molybdenum Co., Ann Arbor, MI, 1982; (b) M. Draganjac, E. Simhon, L. T. Chan, M. Karatzidis, N. C. Baenziger, and D. Coucouvanis, *Inorg. Chem.*, **21**, 3322 (1982); (c) W. K. Miller, R. C. Haltiwanger, M. C. Van Derveer, and M. Rakowski DuBois, *Inorg. Chem.*, **22**, 2973 (1983) and references therein.
(3) A. Müller, E. Diemann, R. Jostes, and H. Bogge, *Angew. Chem., Int. Ed. Engl.*, **20**, 934 (1981).
(4) W.-H. Pan, M. E. Leonowicz, and E. I. Stiefel, *Inorg. Chem.*, **22**, 672 (1983).
(5) R. Kebabcioglu and A. Müller, *Chem. Phys. Lett.*, **8**, 59 (1971).
(6) D. E. Onopko and S. A. Titov, *Opt. Spectrosc. (Engl. Transl.)*, **47**, 185 (1979).
(7) F. W. Kutzler, C. R. Natoli, D. K. Misemer, S. Doniach, and K. E. Hodgson, *J. Chem. Phys.*, **73**, 3274 (1980).
(8) K. Liang et al., to be submitted for publication.
(9) (a) A. Müller and E. Diemann, *Chem. Phys. Lett.*, **9**, 369 (1971); (b) S. S. L. Surana, S. P. Tandon, W. O. Nolte, and A. Müller, *Can. J. Spectros.*, **24**, 18 (1979).
(10) J. Bernholc and N. A. W. Holzwarth, *J. Chem. Phys.*, **81**, 3987 (1984).
(11) R. Hoffman, *J. Chem. Phys.*, **39**, 1397 (1963).
(12) A. R. Williams and U. von Barth in "Theory of the Inhomogeneous Electron Gas", S. Lundqvist and N. H. March, Eds., Plenum Press, New York, 1983.
(13) D. R. Hamann, *Phys. Rev. Lett.*, **42**, 662 (1979).
(14) J. Bernholc and N. A. W. Holzwarth, *Phys. Rev. Lett.*, **50**, 1451 (1983).

0020-1669/85/1324-1323$01.50/0

Table I. Gaussian Decay Constants Used in the MoS_4^{2-} and $Mo_3S_9^{2-}$ Calculations for the Wave Function, Charge, and Exchange Basis Sets (au)[a]

orbital basis	charge basis	exchange basis
	Mo	
0.04 s,r^2s,p,d	0.15 s,r^2s,p,d	0.025 s
0.14 s,r^2s,p,d	0.4 r^2s,d	0.085 s
0.45 s,r^2s,p,d	0.9 r^2s,d	0.33 s,r^2s,p,d
1.33 s,r^2s,p,d	1.4 s,r^2s,p,d	1.25 s,r^2s,p,d
	3.0 s,r^2s,p,d	
	S	
0.085 s,p	0.2 s	0.065 s
0.25 s,p	0.4 s	0.13 s
0.8 s,r^2s,p,d	0.8 s,r^2s,p,d	0.26 s,r^2s,p,d
1.17 s,p	1.3 s	0.43 s
	2.5 s	0.83 s

[a] Hermite Gaussians were used.

Within local density theory[15] one solves the effective equations (in Rydbergs)

$$-\nabla^2\psi_i + \left[\int \frac{2\rho(\mathbf{r}')}{|\mathbf{r}-\mathbf{r}'|}\,d\mathbf{r}' + V_n(\mathbf{r}) + \mu_{xc}(\rho)\right]\psi_i = \epsilon_i\psi_i \qquad (1)$$

$$i = 1, \ldots, \mathbf{r}$$

where ψ_i's denote effective one-electron wave functions with corresponding eigenvalues ϵ_i. The brackets enclose representations of the various contributions to the effective one-electron potential. Within the brackets, the first term is the classical electron–electron repulsion, with $\rho(\mathbf{r})$ being the total electronic charge density, $V_n(\mathbf{r})$ is the total nuclear potential of the atoms, and the last term represents the many-body interactions. It accounts for both exchange and correlation contributions and is thus called the exchange-correlation potential. This potential depends only on the charge density ρ. The functional form of μ_{xc} is determined entirely from electron-gas calculations. In this work the potential of Vosko et al.[16] has been used.

Pseudopotentials (effective core potentials) were used to represent the electron–ion interaction, whereby only valence electrons enter the calculations. These pseudopotentials were projected (once and for all) from first-principles atomic calculations.[17] With the use of pseudopotentials, the wave functions in (1) become pseudo wave functions, which are nodeless but match exactly the real valence wave functions beyond a matching radius, typically much smaller than half of a homonuclear bond length. The atomic eigenvalues are exactly reproduced. The ρ in (1) becomes the total pseudocharge density, and V_n becomes the sum of ionic pseudopotentials.

As a result of the above constraints on the pseudo wave functions, the pseudopotentials are angular momentum dependent. Their effect on the pseudo wave function ψ is

$$V_{ps}\psi = \sum_l V_{ps,l}(r)\, P_l\psi \qquad (2)$$

where P_l projects the appropriate l component from the pseudo wave functions.

The wave functions in (1) were expanded in Gaussian orbitals; the charge density was fitted to an auxiliary set of Gaussian functions. The fitting has the advantage of reducing the well-known N^4 dependence of the computational effort on the number of functions in the wave function basis to N^3.

The fitting procedure was variational,[18] which makes it possible to evaluate the first-order error in total energy induced by the fitting. This error was carefully monitored during the calculations and found small, indicating high quality of the fitting basis.

The equations (1) become the matrix equation

$$\mathbf{HC} = \epsilon\mathbf{SC} \qquad (3)$$

where **H** and **S** are the Hamiltonian and overlap matrices, respectively, ϵ is a column of eigenvalues, and **C** is the eigenvector matrix. The solution of this generalized eigenvalue problem yields eigenvectors that are orthonormal.

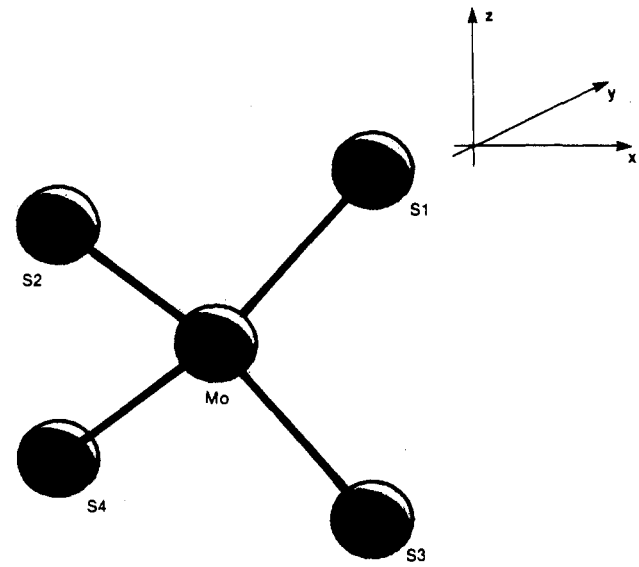

Figure 1. Perspective view of the tetrahedral MoS_4^{2-} anion. The insert defines the direction of the coordinate axes used in the text.

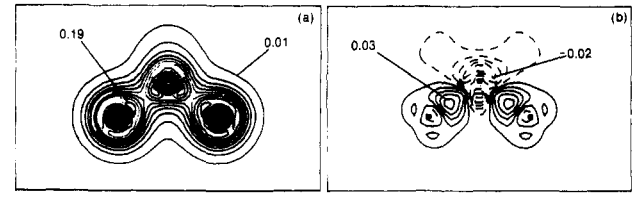

Figure 2. Contour map of (a) the charge density in MoS_4^{2-} and (b) the difference between this charge and the superposition of charges of neutral atoms. The plotting plane contains the Mo and two of the S atoms.

The exchange-correlation potential must be evaluated numerically. It was also fitted to an auxiliary set of Gaussian functions. Once fitted, its matrix elements can be evaluated analytically, as are all the other matrix elements entering eq 3.

The basis sets used for fitting the charge density and the exchange-correlation potential consisted of atom-centered functions of s, p, and d symmetry. The nonspherical and non-muffin-tin effects were thus included.

In the wave function basis we have used four Gaussian exponents per atom. In the charge-fitting basis we have used six exponents for molybdenum and five for sulfur. The exchange basis consisted of four exponents for the molybdenum and five for sulfur. Table I lists the actual decay constants and the angular symmetries.

Both MoS_4^{2-} and $Mo_3S_9^{2-}$ are doubly negatively charged and exist only in a charge-balanced solution or in an ionic crystal where the negative charge is screened by the surrounding medium. We have simulated this effect by scaling the total electron–electron repulsion to compensate for the screening charge.[10]

The calculations were started with the superposition of atomic charges and iterated to self-consistency in order to account for the electronic relaxation and charge redistribution.

The optical transition energies for MoS_4^{2-} were calculated by a variant of Slater's transition-state technique. Assuming that the transition is from the ith to the jth eigenstate, with ground-state occupations n_i and n_j, the transition energy is

$$E(n_i - 1, n_j + 1) - E(n_i, n_j) = \int_0^1 [\epsilon_j(n_j + x) - \epsilon_i(n_i - x)]\,dx \simeq \tfrac{1}{4}[\epsilon_j(n_j) - \epsilon_i(n_i)] + \tfrac{3}{4}[\epsilon_j(n_j + \tfrac{2}{3}) - \epsilon_i(n_i - \tfrac{2}{3})] \qquad (4)$$

where E denotes the total energy of the system, $\epsilon_i(n_i)$ is the (self-consistent) eigenvalue i as a function of occupation number n_i, and we have used Janak's theorem[19] $\partial E/\partial n_i = \epsilon_i$. The formula (4) is correct up to the third derivatives of ϵ with respect to n_i. The spin-restricted transition-state results were 0.05–0.2 eV larger than the difference between the ground-state eigenvalues. For $Mo_3S_9^{2-}$, where the delocalization of the states involved in the transition is greater, the transition energies were estimated from the difference in eigenvalues in the self-consistent

(15) P. Hohenberg and W. Kohn, *Phys. Rev. B*, **136**, B864 (1964); W. Kohn and L. J. Sham, *Phys. Rev.*, **140**, A1133 (1965).
(16) S. H. Vosko, L. Wilk, and M. Nusair, *Can. J. Phys.*, **58**, 1200 (1980).
(17) G. Kerker, *J. Phys. C*, **13**, L189 (1980).
(18) B. I. Dunlap, J. W. D. Connolly, and J. R. Sabin, *J. Chem. Phys.*, **71**, 3396 (1979).
(19) J. F. Janak, *Phys. Rev. B*, **18**, 7165 (1978).

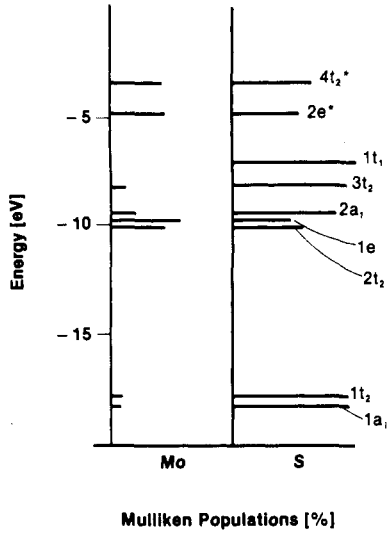

Figure 3. Energy level diagram for MoS_4^{2-} and Mulliken populations for the Mo and the S atoms. For each energy level, the length of the line in the panel is proportional to the relative Mulliken population of this group of atoms.

ground-state calculation. Because of this greater delocalization, we expect that the transition-state calculation would increase these energies by less than 0.15 eV.

III. MoS_4^{2-}

The well-known MoS_4^{2-} anion consists of a central molybdenum atom surrounded tetrahedrally by sulfur atoms (Figure 1) at 2.18 Å.[20]

In Figure 2a we display the pseudocharge density in a plane that includes the molybdenum and two of the four sulfur atoms. The Mo–S bond is found to be only partially ionic with a large covalent component. The difference between the charge of MoS_4^{2-} and the superposition of charges of neutral atoms is shown in Figure 2b. The extra charge localizes mainly in the region of the Mo–S bonds, and the charge transfer from the molybdenum atom to the sulfur atoms is relatively small (notice the different contour spacing in parts a and b of Figure 2). This result is confirmed by the Mulliken populations of 6.24 valence electrons on the molybdenum atom and 6.44 valence electrons on each of the sulfur atoms. The neutral atoms would have 6.0 electrons, and since MoS_4^{2-} is doubly negatively charged, the negative charges of −0.24 and 4(−0.44) add to −2.0 electrons. The small fractional charges are in reasonable agreement with earlier Xα calculations[6] and are consistent with Pauling's electroneutrality principle. The population of the centrally located Mo atom, however, may be somewhat overestimated, due to effects of a large basis set, which includes long-range functions centered on the Mo atom.[21]

We now turn to the eigenstates of MoS_4^{2-}. In Figure 3 we show the energy level diagram together with the Mulliken populations for each level. These energy levels should be compared with the atomic eigenvalues, which are −17.2 and −7.2 eV for the sulfur atom's 3s and 3p, respectively, and −4.3, −4.0, and −1.1 eV for the 5s, 4d, and 5p of the molybdenum atom, respectively.

The lowest four levels are the sulfur 3s orbitals split by the molecular field into an $1a_1$ and a $1t_2$ levels. The molybdenum atom's admixture into these orbitals is very small.

The sulfur atoms interact with Mo primarily via their 3p orbitals. In the tetrahedral symmetry the sulfur 3p levels split into an a_1, e, t_1, and two t_2 levels. The molybdenum orbitals split into an $a_1(s)$, $t_2(d)$, e(d), and another $t_2(p)$. The energetically much higher Mo 5p orbitals contribute only weakly to the occupied or low-lying unoccupied molecular orbitals. The Mo–S bonding interactions occur within a_1, t_2, and e symmetries.

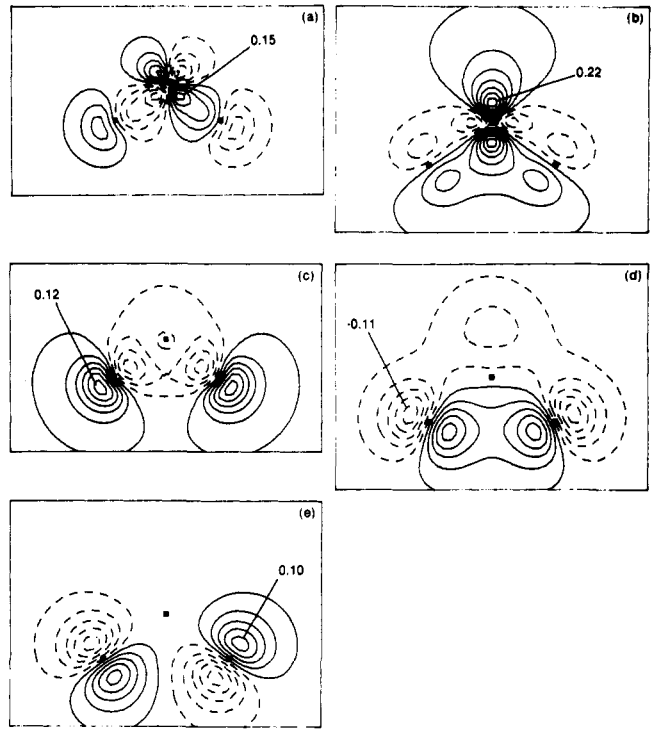

Figure 4. Contour maps of the occupied MO's in MoS_4^{2-} originating from the Mo 4d and 5s and S 3p orbitals: (a) $2t_2$ state at −10.05 eV; (b) 1e orbital at −9.8 eV; (c) $2a_1$ orbital at −9.4 eV; (d) $3t_2$ orbital at −8.1 eV; (e) $1t_1$ orbital at −7.1 eV. See text. The plotting plane is the same as in Figure 2.

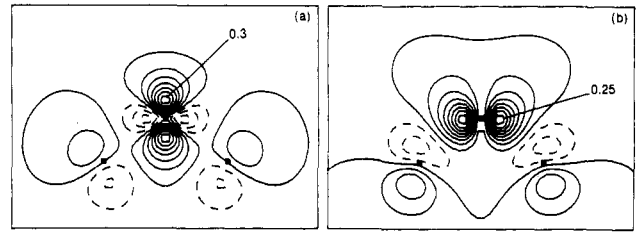

Figure 5. Contour maps of the lowest unoccupied orbitals in MoS_4^{2-} anion: (a) 2e* orbital at −4.8 eV; (b) $4t_2$* orbital at −3.3 eV. See text. The plotting plane is the same as in Figure 2.

The lowest Mo–S bonding level is at −10.05 eV and of t_2 symmetry (Figure 4a). This level consists of Mo d(xy), d(xz), and d(yz) orbitals forming σ bonds with the sulfur atoms. Next lowest is the 1e level of −9.8 eV (Figure 4b). In this level, as is typical for molecules of tetrahedral symmetry, the Mo d(z^2) and d($x^2 - y^2$) orbitals form shared three-center π–σ bonds with the sulfur 3p orbitals. The last filled level with significant Mo admixture is the $2a_1$ orbital at −9.4 eV. It is mainly composed of a fully symmetric combination of sulfur 3p orbitals pointing toward the Mo and interacting with the Mo 5s orbital (Figure 4c). The top two occupied levels at −8.1 eV ($3t_2$) and −7.1 eV ($1t_1$) involve weak interactions between the sulfur 3p levels (Figure 4d,e). The −8.1-eV level has also a small admixture of Mo 5p orbitals. Although the sulfur atoms are 3.55 Å apart, the splitting between the S–S weakly bonding ($3t_2$) and the S–S weakly antibonding ($1t_1$) orbitals is still 1 eV. These distant sulfur–sulfur interactions are also present in other, larger Mo–S complexes (ref 10 and 25 and text below).

The highest occupied molecular orbital is the $1t_1$ level. This orbital has, by symmetry, no Mo content. The interaction of MoS_4^{2-} with acceptor orbitals would therefore primarily involve the sulfur atoms.

If the molecule were neutral, the $1t_1$ orbital would contain two holes. Since the calculated HOMO–LUMO gap is rather large

(20) M. G. Kanatzidis and D. Coucouvanis, *Acta Crystallogr., Sect. C: Cryst. Struct. Commun.*, **C39**, 835 (1983).

(21) In the interpretation of Mulliken populations one should also note that while the charge density is determined very accurately in the present calculation, the populations, which assign charges to the individual atoms, are necessarily weakly basis set dependent.

Table II. Assignments of the Optical Excitations and the Calculated Transition Energies in MoS_4^{2-} (10^3 cm^{-1})[a]

	ν_1		ν_2		ν_3
expt[22]		21.3		31.3	41.2
present work	$1t_1 \rightarrow 2e^*$	20.2	$3t_2 \rightarrow 2e^*$	28.2	$3t_2 \rightarrow 4t_2^*$ 39.5
		(18.3)		(27.4)	(38.7)
			$1t_1 \rightarrow 4t_2^*$	31.4	
				(29.8)	
SW-Xα[6]	$1t_1 \rightarrow 2e^*$	15.3	$1t_1 \rightarrow 4t_2^*$	28.2	$2t_2 \rightarrow 2e^*$ 31.4
	$3t_2 \rightarrow 2e^*$	20.2	$3t_2 \rightarrow 4t_2^*$	33.9	$2a_1 \rightarrow 2e^*$ 38.7
SW-Xα[7]	$3t_2 \rightarrow 2e^*$	21.8	$1t_1 \rightarrow 4t_2^*$	27.4	$1e \rightarrow 4t_2^*$ 44.4
SCCC[5]	$1t_1 \rightarrow 2e^*$	25.8	$1t_1 \rightarrow 4t_2^*$	33.9	$3t_2 \rightarrow 2e^*$ 39.5

[a] The numbers in parentheses denote ground-state results.

(2.3 eV), the doubly charged state is, as expected, strongly preferred.

The lowest unoccupied molecular orbital is the antibonding 2e* level at −4.8 eV (Figure 5a). This is the antibonding partner to the 1e level at −9.8 eV and contains a greater portion of the metal orbitals than its bonding partner. The Mo–S $4t_2^*$, σ^* antibonding level is 1.4 eV higher, at −3.3 eV (Figure 5b). These are the two principal acceptor orbitals. They define a Δ_t value of 1.4 eV. This value is in the range expected for the $E(t_2) - E(e)$ splitting in a tetrahedral ligand field of sulfur donors.[9] It should be compared to the 1.24-eV difference between the first two absorption peaks in MoS_4^{2-}.[22]

The optical absorption bands in MoS_4^{2-} are at 21 300, 31 300, and 41 200 cm^{-1} (2.64, 3.88, 5.11 eV).[22] Within this energy range, the orbitals that may be involved in the transitions are the $2t_2$, 1e, $2a_1$, $3t_2$, and $1t_1$ as the initial states and the 2e* and $4t_2^*$ as the final ones. We find the lowest excitation to be a charge-transfer band $1t_1 \rightarrow 2e^*$ in agreement with most previous theoretical[5,6] and experimental[9,22,23] work (see Table II). For the higher bands, our assignments differ from those proposed previously. We attribute the 31 300-cm^{-1} band to both the $1t_1 \rightarrow 4t_2^*$ and $3t_2 \rightarrow 2e^*$ transitions. The third transition is assigned to $3t_2 \rightarrow 4t_2^*$. The $2t_2 \rightarrow 2e^*$ transition is too high (42 700 cm^{-1}) since the local density method underestimates excitation energies[13] (as is also evident in Table II). The $2a_1 \rightarrow 4t_2^*$ and $1e \rightarrow 2e^*$ transitions are forbidden, and other transitions are even higher in energy. The above transitions are thus the only possible ones. Our assignments and calculated transition energies are compared with the results of previous work in Table II. The Slater transition-state calculations have raised these energies by 400–1600 cm^{-1}, compared to the differences in eigenvalues.

The differences between the first and second and between the second and third band each define Δ_t. The fact that these differences are very close to 10 000 cm^{-1} (1.24 eV) in each case lends further support to the proposed assignments.

IV. $Mo_3S_9^{2-}$

The $Mo_3S_9^{2-}$ ion was recently synthesized from MoS_4^{2-}.[4] The reaction proceeds thermally in solution and likely follows a multistep pathway.[4] We ultimately seek to understand this conversion from as fundamental a viewpoint as possible. The present results, however, address only the initial and final states. In this section, we focus on the electronic properties of $Mo_3S_9^{2-}$.

Structural Considerations. The atomic coordinates of $Mo_3S_9^{2-}$ are known experimentally from the crystal structure[4] of $[P(C_6H_5)_4]_2Mo_3S_9$. The $Mo_3S_9^{2-}$ anion has approximately C_{2v} symmetry. Since the constraints of crystal packing can introduce distortions, and the deviations from the full C_{2v} symmetry are small,[4] we have used atomic coordinates corresponding to the ideal geometry. These coordinates are given in Table III.

In Figure 6 we show a perspective view of $Mo_3S_9^{2-}$. The anion consists of two tetrathiomolybdate units bridged by a five-coordinated Mo in a square-pyramidal arrangement. The Mo-

Table III. Atomic Coordinates of the $Mo_3S_9^{2-}$ Anion Used in the Calculation (Å)

atom	x	y	z
Mo1	−2.88	0	−0.64
Mo2	0	0	0
Mo3	2.88	0	−0.64
S1	−4.08	0	−2.40
S2	−4.08	0	1.17
S3	−1.51	−1.75	−0.62
S4	−1.51	1.75	−0.62
S5	0	0	2.09
S6	1.51	−1.75	−0.62
S7	1.51	1.75	−0.62
S8	4.08	0	−2.40
S9	4.08	0	1.17

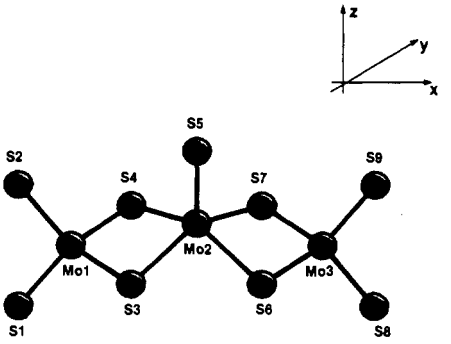

Figure 6. Perspective view of the $Mo_3S_9^{2-}$ anion. The insert defines the direction of the coordinate axes used in the text.

(end)–S(terminal) distances are shorter than in MoS_4^{2-} (2.13 vs. 2.18 Å), while the Mo(end)–S(bridging) distances are longer (2.23 vs. 2.18 Å). For the fivefold-coordinated Mo(center) the differences in the bond lengths are even greater, with the Mo–S(top) being 2.09 Å and Mo–S(bridging) averaging 2.39 Å. The Mo(end)–Mo(center)–Mo(end) angle of 155° may indicate possible Mo–Mo and/or S–S sideways interaction along the x axis (S3–S6 and S4–S7). However, in a dinuclear grouping containing edge-shared tetrahedral and square-pyramidal Mo units with the square-pyramidal Mo atom lying 0.6 Å above the plane of the four basal ligands and with no Mo–Mo bonding, the dihedral angle is also 155°. Thus, on a solely structural basis there is no reason to invoke M–M bonding.

Overall Charge Distribution. The variation in Mo–S bond distances is indicative of the relative bond strengths and is reflected in the charge distribution of the molecule. In Figure 7 we show contour maps of the charge density and of the difference between this charge and the superposition of atomic charges. The first plotting plane (Figure 7a,b) contains the three molybdenum atoms and all the terminal sulfur atoms. The charge distribution in Mo–S(terminal) bonds is very similar to that of MoS_4^{2-}. The difference between this charge and the superposition of charges of neutral atoms (Figure 7b) shows that the charge transfer (from molybdenum to sulfur) is relatively small. Since the strongest bond contains the greatest amount of bonding charge, Figure 7b shows that the strongest Mo–S(terminal) bond is the one involving the central molybdenum, in agreement with the experimental bond

(22) R. H. Petit, B. Briat, A. Müller, and E. Diemann, *Mol. Phys.*, **27**, 1373 (1974).
(23) (a) R. J. H. Clark, T. J. Dines, and M. L. Wolf, *J. Chem. Soc., Faraday Trans.*, **278**, 679 (1982); (b) E. Koniger-Ahlborn and A. Müller, *Spectrochim. Acta, Part A*, **33A**, 273 (1977).

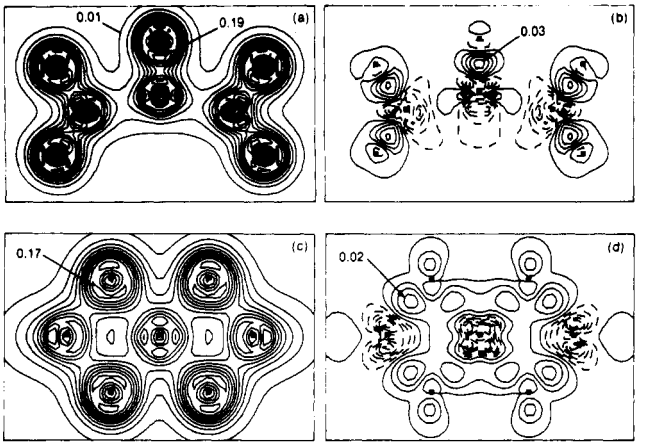

Figure 7. Contour maps of the charge density (a and c) and the difference density (b and c) in $Mo_3S_9^{2-}$. The plotting plane (xz) in (a) and (b) contains the three Mo atoms and all the terminal sulfur atoms. The plotting plane in (c) and (d) is located 0.32 Å below the central Mo atom and is parallel to the xy plane. See text.

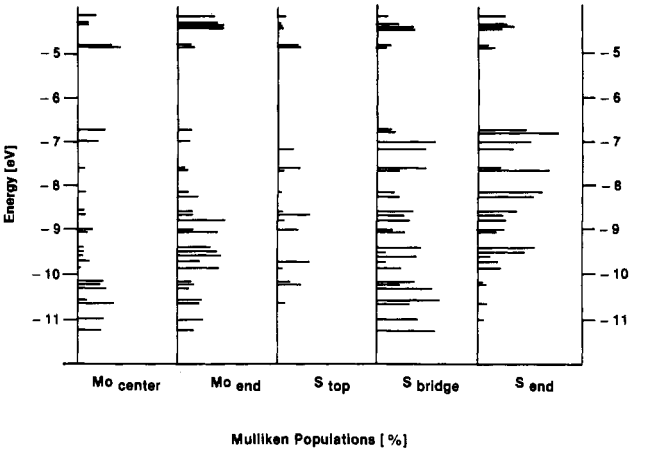

Figure 8. Energy level diagram for the $Mo_3S_9^{2-}$ anion and Mulliken populations for the central and the end Mo atoms and the top, the bridging, and the end S atoms. For each energy level, the length of the line in the panel is proportional to the relative Mulliken population of this group of atoms (the sulfur 3s levels are not shown).

distances. The central Mo shows some delocalization of the charge density in the direction of the other molybdenum atoms. This delocalization is due to charge movement from the central molybdenum atom in the IV oxidation state to the end molybdenum atoms in the VI oxidation state. We will support this contention below when we discuss individual orbitals.

The charge density and the difference density of the Mo–S(bridging) bonds is shown in Figure 7c,d. Since the central Mo is located 0.64 Å above the xy plane in which the end molybdenum atoms and the bridging sulfur atoms lie, we have placed the plotting plane 0.32 Å below the central Mo and parallel to the xy plane. In this way the relative strengths of the two types of the bridging bonds can be compared. The Mo(end)–S(bridging) bond contains more electron density and is thus stronger, again in agreement with the bond distances. The square-pyramidal MoS_5 central fragment has the strongest and the four weakest Mo–S bonds. The external MoS_4^{2-} units have two weaker terminal and two stronger bridging bonds than the central Mo. We note also the significant charge enhancement behind the bridging sulfur atoms along the y axis outside of the chelate ring. It is due to the three-center S–Mo–S bonding or "through-metal" bonding in several of the molecular orbitals (vide infra).

The Mulliken populations are 6.41 and 6.24 valence electrons for the central and end molybdenum atoms, respectively, and 6.21, 6.07, and 6.00 valence electrons for the end, bridging, and top sulfur atoms, respectively. Since the neutral atoms have Mulliken populations of 6.0 valence electrons, these populations are consistent with Pauling's electroneutrality principle (as is the case in MoS_4^{2-}). In comparison with the Mo and S populations in tetrathiomolybdate (6.24 and 6.44 electrons, respectively), one should take into account that the excess negative charge in MoS_4^{2-} is 0.40 electron/atom, while in $Mo_3S_9^{2-}$ it is only 0.17 electron/atom. The difference in populations between the end and bridging sulfur atoms shows, however, that the bridging sulfur atoms in the two MoS_4^{2-} fragments donate charge to the central Mo atom, while the end molybdenum atoms accept charge from both sulfur atoms *and* from the *central* Mo atom (see below).

Energy Levels. We now turn to the individual molecular orbitals of the system. In Figure 8 we show the energy level diagram along with the Mulliken populations of each level. The sulfur 3s orbitals, which are lower in energy and not involved in bonding, are not shown. The bonding, as in MoS_4^{2-}, occurs primarily between sulfur 3p and Mo 4d and 5s orbitals. The individual molecular orbitals are strongly delocalized and extend through large parts of the molecule. This delocalization is typical of Mo–S complexes and has been observed in other molecules as well.[10,24] The delocalization can be best illustrated by examining the Mulliken atomic populations for the various molecular levels (Figure 8).

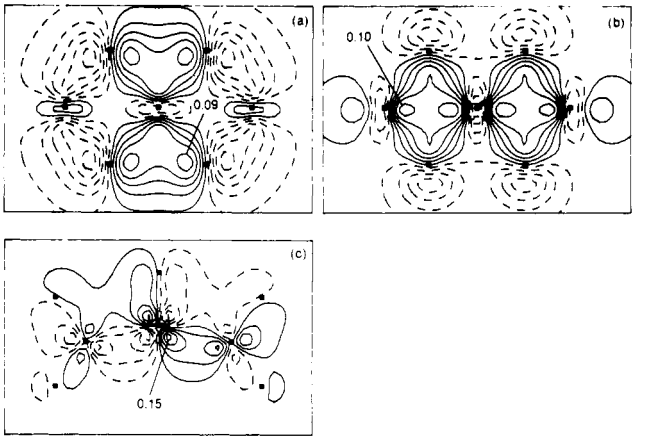

Figure 9. Contour maps of the bonding orbitals that involve all three Mo atoms: (a) at −11.25 eV (plotting plane as in Figure 7c); (b) at −11 eV (plotting plane as in Figure 7a); (c) at −10.62 eV (plotting plane as in Figure 7a). See text.

The $Mo_3S_9^{2-}$ anion has 37 occupied valence levels. Apart from the nine sulfur 3s orbitals, the remaining levels group energetically into 20 Mo–S bonding levels (the lowest), followed by three S–S weakly bonding and three weakly antibonding S–S levels, and two mixed levels containing an antibonding S–S level and a nominally nonbonding Mo orbital. Several of the levels can be viewed as originating from the MoS_4^{2-} fragments. These orbitals are relatively unchanged as compared to the free tetrathiomolybdate (see section III). In the following we analyze the $Mo_3S_9^{2-}$ orbitals in detail.

Mo–S Bonding Levels. The four lowest lying Mo–S bonding levels involve all three molybdenum atoms and the bridging sulfur atoms. The orbital at −11.25 eV (Figure 9a) consists of Mo–S bonds and is stabilized by the S–S(side) (i.e., S_3–S_6 and S_4–S_7) σ bonding in the x direction mediated by d orbitals on the central molybdenum atom. Another orbital with a similar bonding pattern is at −10.60 eV. The bridging sulfur atoms also mediate a metal–metal interaction in the level at −11 eV (Figure 9b), where strong multicenter bonds are formed with the Mo(end) and Mo(center) atoms utilizing $d(x^2-y^2)$ and $d(z^2)$ orbitals, bridged by $p(y)$ orbitals on the sulfur atoms. Finally, the last of the low-lying orbitals involving all three molybdenum atoms (at −10.62 eV) consists of a strong central Mo $d(xz)$ component, Mo(end) $d(x^2-y^2)$, $d(z^2)$, and $d(xz)$ orbitals (Figure 9c), and has a significant admixture of the bridging and top sulfur atomic orbitals in the plane perpendicular to the figure.

(24) Similar effects were observed in $Mo_2O_2S_2(S_2)_2^{2-}$[10] and in $Mo_2S_2S_2(S_2)_2^{2-}$.[25]

(25) J. Bernholc and E. I. Stiefel, to be submitted for publication.

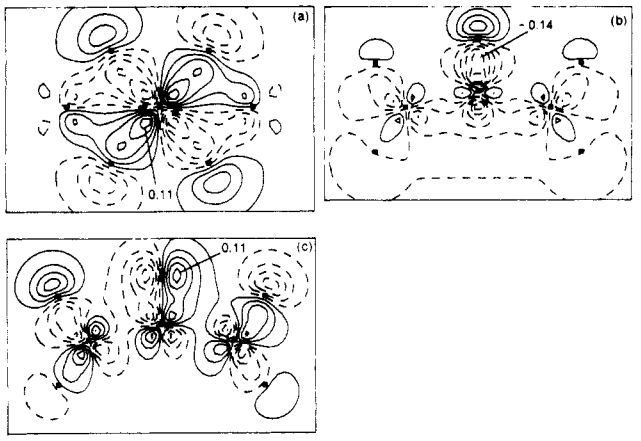

Figure 10. Contour maps of the bonding orbitals associated with the central Mo: (a) at −10.3 eV (plotting plane as in Figure 7c); (b) at −10.22 eV (plotting plane as in Figure 7a); (c) at −9.0 eV (plotting plane as in Figure 7a). See text.

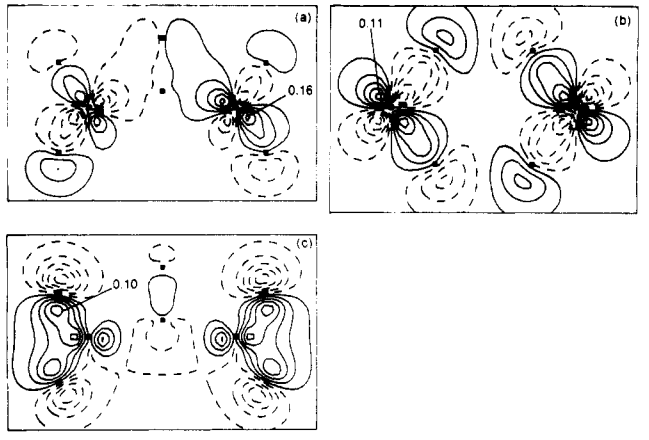

Figure 11. Contour maps of the bonding orbitals associated with the end Mo atoms: (a) at −9.9 eV (plotting plane as in Figure 7a); (b) at −9.6 eV (plotting plane contains the end Mo and the bridging S atoms); (c) at −8.25 eV (plotting plane as in Figure 7a). See text.

The next group of five MO's is associated predominantly with the central Mo. In the lowest of these levels, at −10.3 eV, Mo uses the d(xy) orbital to form σ bonds with the bridging sulfur atoms (Figure 10a). Although there is some admixture of orbitals of the end molybdenum atoms, this admixture is much weaker than that discussed above. The other four levels in this group strongly involve the top sulfur atom. The Mo(center)–S(top) σ-bonding orbital mixes with the Mo(end)–S(end) orbitals, resulting in two levels with roughly equal Mo(center)–S(top) σ-bonding character, at −10.22 and at −9.7 eV. The lower of these is shown in Figure 10b. The Mo(center)–S(top) π-bonding orbitals are located at −10.15 eV and at −9.0 eV. The latter mixes significantly with the Mo(end)–S(end) σ-bonding orbitals (Figure 10c).

The next group of four MO's contain Mo(end)–S(end) σ-bonding levels located at −9.9, −9.5, −9.4, and −8.6 eV. In Figure 11a we show the lowest of these orbitals. Note the similarity to the corresponding orbital of the free MoS_4^{2-} anion (Figure 4a). The bonding to the lower and upper sulfur atoms is however no longer equivalent due to the lower symmetry of the $Mo_3S_9^{2-}$.

The four σ-bonding levels with dominating Mo(end)–S(bridging) character lie at −9.6, −9.38, −9.0, and −8.8 eV. The orbital at −9.6 eV is shown in Figure 11b. Note again the strong similarity with the corresponding MoS_4^{2-} orbital (Figure 4a). The level at −9.38 eV contains an admixture of the central Mo d orbitals, and the level at −9.0 eV has both Mo(end)–S(bridging) and Mo(center)–S(bridging) contributions. In the same energy range (at −8.66 eV) there is also a MO having a strong S(top) p(y) contribution, weakly π bonding to the central Mo, mixed with a Mo(end)–S(bridging) component.

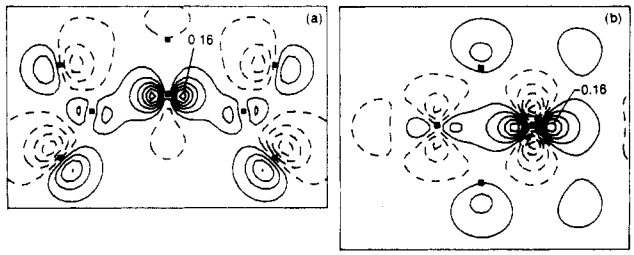

Figure 12. Contour maps of the HOMO at −6.72 eV in (a) the xz plane and (b) the plane containing the Mo1 and Mo2 atoms and parallel to the y axis. See text.

Two of the four S(end)–Mo(end)–S(end) three-center bonding orbitals correspond to the e levels of MoS_4^{2-} (Figure 4b) and lie at −8.25 eV and at −8.14 eV. The lower one is shown in Figure 11c. These are similar to the molecular orbitals involving the bridging sulfur atoms, which, however, are shifted to lower energies by mixing with the Mo(center)-derived ones, and have already been discussed (Figure 9b).

A total of 20 Mo–S bonding levels are thus responsible for the five terminal and eight bridging Mo–S bonds. A strict separation of the various levels into σ and π bonding, however, is not fruitful, due to the large mixing of the σ and π components in the molecular orbitals. This concludes the description of Mo–S bonding levels.

Weakly Interacting Sulfur and Molybdenum Levels. The six levels involving only the sulfur atoms are as follows: two at −7.61 eV (very weak π bonding among end sulfur atoms); one at −7.6 eV (very weak π bonding among the bridging sulfur atoms along the y axis but π^* antibonding sideways along the x axis with some S(top) admixture); one at −7.16 eV (very weakly π^* antibonding among the bridging sulfur atoms but sideways π bonding along the x axis with some S(top) admixture); one at −6.96 eV (π^* antibonding along both x and y directions); one at −6.75 eV (S(end) π^* weakly antibonding). The ordering of the above levels shows that the bonding interactions among the bridging sulfur atoms in the chelating ring (at 3.5 Å) are stronger than the sideways interaction among sulfur atoms belonging to different rings (at 3.02 Å) despite the longer distance. However, since both the weakly bonding and weakly antibonding levels are occupied, there is no net S–S bonding.

The level at −6.75 eV corresponds to one of the components of the triply degenerated t_1 level of MoS_4^{2-} (Figure 4e). We expect two such orbitals from the two MoS_4^{2-} units. However, the symmetric linear combination of the two orbitals mixes strongly with the occupied d($x^2 - y^2$) orbital of the central Mo (the central Mo is Mo^{IV}) to produce two levels at −6.98 eV and at −6.72 eV. The last one is the HOMO. Contour plots of this orbital in the xz plane and in the plane containing the Mo(center) and one of the Mo(end) atoms are shown in parts a and b of Figure 12 respectively. There is significant admixture of Mo(end) orbitals (or the 2e* level; cf. Figure 5a) in this state.

In the formulation in which two MoS_4^{2-} ions act as ligands to the MoS^{2+} central unit; this result confirms the often made claim that MoS_4^{2-} is an acceptor as well as a donor ligand.[1e,3,4] Clearly, the donor orbitals of MoS_4^{2-} are S based while the acceptor levels consist mainly of the empty d levels on MoS_4^{2-}. This metal → metal donor–acceptor binding is likely to be partially responsible for the ability of MoS_4^{2-} to stabilize lower valent metals to which it binds.[1e,26]

The HOMO and the S(end) π^* level at −6.75 eV are split by only 0.03 eV, which is less than the accuracy of the calculations. Since the Mo d($x^2 - y^2$) orbital is relatively inaccessible within the molecule, the S(end)–S(end) π^* orbitals are most likely to act as the frontier donor orbitals in chemical reactions.

Unoccupied Levels. In $Mo_3S_9^{2-}$ the calculated HOMO–LUMO gap is 1.9 eV. The lowest unoccupied molecular orbitals are Mo(center)–S(top) π^*-antibonding orbitals (Figure 13a) at −4.84

(26) D. Coucouvanis, E. D. Simhon, and N. C. Baenziger, *J. Am. Chem. Soc.*, **102**, 6644 (1980).

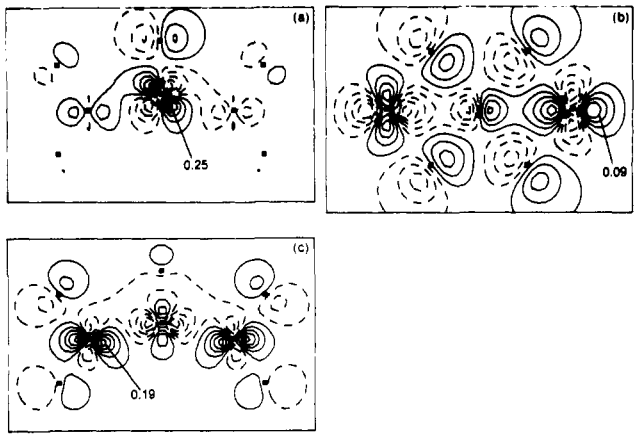

Figure 13. Contour plots of the low-lying unoccupied orbitals of the $Mo_3S_9^{2-}$ anion: (a) at −4.84 eV (the LUMO) (plotting plane as in Figure 7a); (b) at −4.4 eV (plotting plane as in Figure 7c); (c) at −4.18 eV (plotting plane as in Figure 7c). See text.

eV. These MO's are followed by a Mo(end)–S(bridging) π^*-antibonding level (Figure 13b) at −4.4 eV, which is somewhat stabilized by the bonding interactions between the end molybdenum atoms and the Mo(center) 5p orbital. The first of the Mo(end)–S(end) π^*-antibonding levels are at −4.38 and −4.35 eV. The latter of these levels contains an admixture of the Mo(center) d(yz) orbital. This MO is followed by the Mo(end)–Mo(center)–Mo(end) antibonding d($x^2 - y^2$) and d(z^2) levels (Figure 13c) at −4.18 eV. The above MO's are most likely to act as frontier acceptor orbitals. The remaining unoccupied MO's are all above −3.6 eV.

Absorption Spectrum. The absorption bands of $Mo_3S_9^{2-}$ are quite broad with a weak, broad feature at 16 800 cm^{-1} and peaks or shoulders at 21 500, 26 800, 29 400, and 32 200 cm^{-1}.[4] In this spectral range we calculate about 80 allowed or weakly allowed transitions. Each of the peaks or shoulders corresponds to several transitions, making a precise assignment of the spectrum an almost impossible task at the present time. We will, however, list below the transitions that give the strongest contributions to the observed spectrum. Our assignments are based on differences of the self-consistent, spin-restricted eigenvalues and on oscillator strengths calculated from the ground-state wave functions. The transition energies should thus be adjusted upward by 400–1200 cm^{-1} in order to account for transition-state effects. In the assignments we have also taken into consideration the fact that the local density theory generally underestimates excitation energies.[13]

In general, transitions in $Mo_3S_9^{2-}$ can be viewed (1) as within the MoS_4^{2-} ligands, (2) as within the MoS_5 central unit, and (3) as supermolecular.

The weak, broad feature at 16 800 cm^{-1} is attributed to the excitation from the Mo(center) nominally nonbonding d($x^2 - y^2$) orbital and the S(end) weakly π^* orbitals to the Mo(center)–S(top) π^*-antibonding orbitals (LUMOs). The calculated transition energy is 15 300 cm^{-1}, and the oscillator strength for the transition is small, in agreement with experimental observations. Since the LUMOs contain mainly the central Mo d orbitals, this is as close as one can come to a d–d transition in systems as delocalized as these. This transition becomes allowed due to the admixture of the sulfur orbitals in the LUMOs.

The broad, asymmetric peak at 21 500 cm^{-1} is resolved into two lines at 23 000 and 21 200 cm^{-1} in second-derivative spectra.[4] It is clearly of similar energy and assignment as the S → Mo band in MoS_4^{2-}. We find several transitions in this region with relatively large oscillator strengths: from the S(bridging) weakly π^* MO to the LUMO (at 17 200 cm^{-1}) and to the Mo(end)–S(end) π^* orbital (at 21 000 cm^{-1}); from the HOMO and from the S(end) weakly π^* MO to the Mo(end)–S(bridging) π^* MO (at 18 800 and 19 000 cm^{-1}, respectively); from the S(bridging) weakly π bonding but S–S(side) π^* antibonding MO to the LUMO (at 22 000 cm^{-1}); from the lower of the two Mo(center) d($x^2 - y^2$) and S(end) π^* mixed MO's to the three-Mo antibonding orbital (at 22 400 cm^{-1}). Except for the latter transition, which has some metal → metal components, the remaining contributions to the 21 500-cm^{-1} peak involve charge-transfer excitations from S–S weakly π^* states to the Mo–S π^* orbitals in complete analogy to the spectrum of MoS_4^{2-}.

We will now list tentative assignments for the shoulders at higher energies. As before, only transitions with relatively large oscillator strengths are included.

The shoulder at 26 600 cm^{-1} is attributed to the transitions from the S(end) weak π-bonding MO's to the Mo(end)–S(end) π^* orbital (at 26 200 cm^{-1}). This is the equivalent of the $3t_2 \rightarrow 2e^*$ transition in MoS_4^{2-}.

The shoulder at 29 400 cm^{-1} is ascribed to the transition from the HOMO to Mo(end)–S(end) σ^* orbitals (at 28 200 cm^{-1}). Finally, there are three strong transitions in the region of the 32 200-cm^{-1} shoulder: from the HOMO to the next Mo(end)–S(end) σ^* MO (at 30 000 cm^{-1}); from a nonbonding S(top) 3p orbital to the LUMO (at 30 900 cm^{-1}); from the S(bridging) π^* but S–S(side) π-bonding orbital to the Mo(end)–S(bridging) σ^* orbital (at 31 100 cm^{-1}).

Although the above assignments are necessarily approximate and tentative, they nevertheless show that the dominant absorption bands are due primarily to ligand → metal charge-transfer transitions and in most cases correspond to transitions found in MoS_4^{2-}.

V. Summary and Conclusions

In both MoS_4^{2-} and $Mo_3S_9^{2-}$ we have found a relatively small charge transfer from molybdenum to sulfur in the ground states of the molecules when compared to the free atoms. The closeness of the atomic energy levels of sulfur 3p orbitals and molybdenum 4d and 5s levels results in a substantial delocalization of the molecular orbitals.[24] This delocalization is in part responsible for the enormous structural variety found in Mo–S species that in turn may engender their enzymatic and catalytic utility.

For MoS_4^{2-}, our results are qualitatively in agreement with previous Xα calculations.[6,7] The present method, however, does not make approximations to the shape of the molecular potential and therefore gives much more accurate charge density profiles and true local density eigenvalues. These results have led to new assignments of the higher absorption bands. In both MoS_4^{2-} and $Mo_3S_9^{2-}$ the distant sulfur atoms (at 3–3.5 Å) still interact sufficiently to split some of their bonding and antibonding levels by 0.7 eV. However, since both the bonding and the antibonding levels are filled, there is no net S–S bonding.

The general ordering of occupied levels in these systems is as follows: the lowest are the metal–sulfur bonding levels with some degree of metal–metal bonding, followed by the remaining metal–sulfur bonding levels, the sulfur–sulfur (at 3–3.5 Å) weakly bonding ones, the Mo–Mo bonding levels[10,25] (if present), and finally by the sulfur–sulfur weakly antibonding orbitals. Nominally nonbonding Mo orbitals are at energies comparable with the weakly antibonding sulfur levels. The same general ordering is observed in other systems.[10,25]

The lowest unoccupied molecular orbitals are, in the cases we have studied thus far, metal–ligand π^*-antibonding orbitals (i.e., the classical ligand field d levels, but strongly mixed with sulfur p levels).

The near-degeneracy of the nonbonding Mo d orbitals and the weakly antibonding distant sulfur orbitals suggests plausible explanations for the rapid interconversions of MoS species. For example, $MoS_4^{2-} \rightarrow MoS_9^{2-}$,[26,27] $MoS_4^{2-} \rightarrow Mo_2S_{12}^{2-}$,[2b] or $MoS_4^{2-} \rightarrow Mo_2S_8^{2-}$[27] all involve ready intermolecular electron transfer from S to Mo or Mo to S that is facilitated by the closeness of the energy levels.

In MoS_4^{2-}, the highest occupied molecular orbitals are the weakly π^*-antibonding sulfur 3p orbitals. By symmetry, these orbitals have no Mo content. The calculated HOMO–LUMO gap is 2.3 eV.

(27) W.-H. Pan, M. A. Harmer, T. R. Halbert, and E. I. Stiefel, *J. Am. Chem. Soc.*, **106**, 459 (1984).

In $Mo_3S_9^{2-}$ several molecular orbitals correspond directly to orbitals of the MoS_4^{2-} fragments. However, because of its larger size and lower symmetry, the mixing and delocalization of orbitals is much greater.

The highest occupied molecular orbitals in $Mo_3S_9^{2-}$ are π^*-antibonding S(end) orbitals (analogous to the t_1 orbitals in MoS_4^{2-}) and the central Mo $d(x^2 - y^2)$ orbital. The latter is not easily accessible due to the surrounding ligands, making the S(end)–S(end) π^*-antibonding orbital the most probable frontier donor orbital. Since the central Mo $d(x^2 - y^2)$ orbital is occupied by two electrons, the formal oxidation states of molybdenum are Mo(VI) for the end molybdenum atoms and Mo(IV) for the central one. These results are in agreement with earlier assignments.[4] The calculated HOMO–LUMO gap in this system is 1.9 eV. The low-lying acceptor orbitals in $Mo_3S_9^{2-}$ are the Mo(center)–S(top), Mo(end)–S(bridging), and Mo(end)–S(end) π^*-antibonding orbitals. Description of the binding in terms of the two MoS_4^{2-} fragments and the MoS^{2+} central core confirms the idea that MoS_4^{2-} can act as an acceptor as well as a donor ligand.

Acknowledgment. We thank Drs. W.-H. Pan, T. R. Halbert, and S. Harris for useful discussions.

Registry No. MoS_4^{2-}, 16330-92-0; $Mo_3S_9^{2-}$, 95344-47-1.

Contribution from Inorganic Chemistry 1,
Chemical Center, University of Lund, S-221 00 Lund, Sweden

Crystal Structure of Iodo(tetrahydrothiophene)gold(I) at 200 K: A Compound with an Infinite Array of Gold–Gold Bonds

STEN AHRLAND,* BERTIL NORÉN, and ÅKE OSKARSSON

Received April 11, 1984

The crystal structure of $[Au[\overline{S(CH_2)_3CH_2}]I]_\infty$ has been determined from X-ray intensity data collected at 200 K with a CAD4 diffractometer. The space group is orthorhombic, $Pc2_1n$ with $Z = 8$, $a = 8.149$ (2) Å, $b = 11.460$ (4) Å, and $c = 15.956$ (3) Å. The refinement converged to $R = 0.062$. There are two different Au atoms in the asymmetric unit. One coordinates two iodides in an almost linear fashion. Both Au–I distances are 2.565 (2) Å, and the I–Au–I angle is 177.57 (7)°. The other Au atom coordinates two S atoms, also in an almost linear fashion. The Au–S distances are 2.306 (7) and 2.335 (6) Å, respectively, and the S–Au–S angle is 172.4 (2)°. The two Au units are repeated alternately with another throughout the structure, forming zigzag-shaped chains running along *b*, with Au–Au–Au angles 155.46 (4) and 161.25 (4)°. There are only van der Waals bonds between the chains. The Au–Au distances within a chain are very short, 2.967 (2) and 2.980 (2) Å. Since there are no ligand bridges between the gold atoms, these short distances certainly indicate a fairly strong metal–metal bonding. The gold atoms are thus four-coordinated, with the coordination figures most aptly described as very compressed tetrahedra.

Introduction

The monovalent oxidation states of the coinage metals copper, silver, and gold are typically soft acceptors, strongly preferring soft ligands. Consequently, they are preferentially solvated by solvents coordinating via soft donor atoms such as nitrogen and, even more markedly, sulfur. The present investigation is part of an extensive study of the interplay between solvation and complex formation for these acceptors, involving various soft solvents and ligands.[1-4] So far, these investigations have concerned copper(I) and silver(I). Presently, they are extended to gold(I).

Soft solvents, as soft ligands generally do, strongly stabilize the monovalent state of these metals, i.e. the d^{10}-electron configuration, both relative to the metal and to the higher oxidation states. In the case of copper(I), this has been established both for acetonitrile (AN) and for pyridine (py),[1-6] and in the case of gold(I) for AN.[6-8] Also, silver(I) is much less oxidizing in these solvents than in a hard solvent such as water.[1,9] In solvents coordinating via sulfur, softer than nitrogen, the d^{10} configurations should be still more strongly stabilized.

Aliphatic sulfides are good electron donors and should thus be strongly solvating solvents of the soft category. Among these, the cyclic thioether tetrahydrothiophene (THT) has been selected for the present investigation, on account of its favorable liquid range (−96 to +119 °C), ready availability, and ease of purification and handling.

Table I. Crystal Data for Au(THT)I

orthorhombic	space group $Pc2_1n$
$a = 8.149$ (2) Å	mol wt 412.04
$b = 11.460$ (4) Å	$T = 200$ K
$c = 15.956$ (3) Å	μ(Mo Kα) = 239.5 cm^{-1}
$V = 1490.0$ Å^3	ρ(calcd) = 3.673 g cm^{-3}
$Z = 8$	

The solvates and complexes studied previously have been investigated by thermodynamic, structural, and spectroscopic methods.[1-4] The latter methods have been applied both to species in solution and to solids crystallized from the solutions. The present study concerns the structure of a THT solvate of gold(I) iodide, containing the components in the molar ratio Au:I:THT = 1:1:1. The structure turns out to possess several remarkable features; it is moreover completely different from that of the corresponding silver(I) compound of the same stochiometric composition.[10]

Experimental Section

Materials. $[Au[\overline{S(CH_2)_3CH_2}]I]_\infty$ was prepared by treating a gold foil (0.57 g) with a solution of I_2 (0.37 g) in THT (5 mL), at 60–70 °C. After the mixture was cooled to room tempeature, single crystals of the title compound were formed. These were prismatic and light yellow. One of these crystals was used for the collection of the X-ray intensity data. Later on, we observed that the gold foil reacts with the iodine solution even at room temperature, with the formation of beautiful crystals on the metal surface. The same compound was formed irrespective of the mode

(1) Ahrland, S. *Pure Appl. Chem.* **1982**, *54*, 1451–1468.
(2) Nilsson, K.; Oskarsson, Å. *Acta Chem. Scand., Ser. A* **1982**, *A36*, 605–610.
(3) Nilsson, K.; Oskarsson, Å. *Acta Chem. Scand., Ser. A* **1984**, *A38*, 79–85.
(4) Ahrland, S.; Nilsson, K.; Tagesson, B. *Acta Chem. Scand., Ser. A* **1983**, *A37*, 193–201.
(5) Hemmerich, P.; Sigwart, C. *Experientia* **1963**, *19*, 488–489.
(6) Bergerhoff, B. *Z. Anorg. Allg. Chem.* **1964**, *327*, 139–142.
(7) Goolsby, A. D.; Sawyer, D. T. *Anal. Chem.* **1968**, *40*, 1978–1983.
(8) Bravo, O.; Iwamoto, R. T. *Inorg. Chim. Acta* **1969**, *3*, 663–666.
(9) Kolthoff, I. M.; Chantooni, M. K., Jr. *J. Phys. Chem.* **1972**, *76*, 2024–2034.
(10) Norén, B.; Oskarsson, Å., to be submitted for publication.

0020-1669/85/1324-1330$01.50/0